the precise mechanism of their tolerance to beta irradiation remains unknown. However, when the relationship between ^{201}Tl uptake and S-phase fraction is taken into consideration, two possibilities are hypothesized. First, in vitro studies have proven that the cells in the late S-phase are more radioresistant than they are in other phases of cell cycle (*26,27*). Higher ^{201}Tl uptake indicates that radioresistant cells are more abundant in the tumor. Second, the cells in S-phases have more proliferating activity and may be less dependent on TSH regulation. Therefore, serum TSH may not be a strong stimulator in increasing radioiodine uptake with high ^{201}Tl uptake tumor.

CONCLUSION

Thallium-201 does not reflect thyroid function. There is a size dependency for planar ^{201}Tl image to detect metastatic tumors. Therefore, evaluation of ^{201}Tl uptake is difficult in functioning but small or radiographically silent metastases. Thallium-201 is not a perfect alternative to radioiodine. However, in the case of a radiographically measurable tumor, ^{201}Tl scintigraphy has a predictive value for the efficacy of radioiodine therapy. It can detect metastatic thyroid tumors and can give physicians better discretion in managing metastatic thyroid carcinoma.

REFERENCES

1. Harbert JC. *Nuclear medicine therapy.* New York: Thieme Medical Publishers Inc.; 1987:57.
2. Schlumberger M, Tubina M, Vatharie F, et al. Long-term results of treatment of 283 patients with lung and bone metastases from differentiated thyroid carcinoma. *J Clin Endocrinol Metab* 1986;63:960–967.
3. Maxson HR III, Smith HS. Radioiodine-131 in the diagnosis and treatment of metastatic well differentiated thyroid cancer. *Endocrinol Metab Clin North Am* 1990;19:685–718.
4. Eshima K, Izumi M, Tominaga T, et al. The significance of ^{131}I treatment of metastatic thyroid carcinoma. *Int J Oncol* 1993;2:877–882.
5. Hoefnagel CA, Delprat CC, Marcuse HR, de Vijlder JJM. Role of thallium-201 total body scintigraphy in follow up of thyroid carcinoma. *J Nucl Med* 1986;27:1854–1857.
6. Brendel AJ, Guyot M, Jeandit R, Lefort G, Manciet G. Thallium-201 imaging in the follow up of differentiated thyroid carcinoma. *J Nucl Med* 1986;27:1854–1857.
7. Ramanna L, Waxman A, Braustein G. Thallium-201 scintigraphy in differentiated thyroid cancer: comparison with radioiodine scintigraphy and serum thyroglobulin determinations. *J Nucl Med* 1991;32:441–446.
8. Charkes ND, Vitti RA, Brooks K. Thallium-201 SPECT increases detectability of thyroid cancer metastases. *J Nucl Med* 1990;31:147–153.
9. Dadparvar S, Krishna L, Brady LW, et al. The role of iodine-131 and thallium-201 imaging and serum thyroglobulin in the follow-up of differentiated thyroid carcinoma. *Cancer* 1993;71:3767–3773.
10. Lorberboym M, Murthy S, Mechanick JI, Bergman D, Morris JC, Kim K. Thallium-201 and iodine-131 scintigraphy in differentiated thyroid carcinoma. *J Nucl Med* 1996;37:1487–1491.
11. Nakada K, Katoh C, Kanegae K, et al. The role of ^{201}Tl scintigraphy in evaluating proliferative activity in thyroid neoplasms. *Ann Nucl Med* 1996;10:41–48.
12. Nemic J, Rohling S, Zamarazil V, Pohunkova D. Comparison of the distribution of diagnostic and thyroablative ^{131}I in the evaluation of differentiated thyroid cancers. *J Nucl Med* 1979;20:92–97.
13. Bachandran S, Sayle BA. Value of thyroid carcinoma imaging after therapeutic dose of radioiodine. *Clin Nucl Med* 1981;6:162–167.
14. Waxman A, Ramanna L, Chapman N, et al. The significance of ^{131}I scan dose in patients with thyroid cancer: determination of ablation: concise communication. *J Nucl Med* 1981;22:861–865.
15. Britten JS, Blamk M. Thallium activation of the (NA^+-K^+) activated ATPase of rabbit kidney. *Biochim Biophys Acta* 1968;159:160–166.
16. Takekawa H, Itoh K, Abe S, et al. Thallium-201 uptake, histopathological differentiation and Na-K ATPase in lung adenocarcinoma. *J Nucl Med* 1996;37:955–958.
17. Muranaka A. Accumulation of radioisotopes with tumor affinity. II. Comparison of the tumor accumulation of gallium-67 citrate and thallium-201 chloride in vitro. *Acta Med Okayama* 1981;35:85–101.
18. Itoh Y, Muranaka A, Harada T, Matsuda A, Yokobayashi T, Terashima H. Experimental study of tumor affinity of ^{201}Tl-chloride. *Eur J Nucl Med* 1978;3:81–86.
19. Sandrock D, Merino MJ, Norton A, Neumann RD. Ultrastructural histology correlated with results of thallium-201/technetium-99m parathyroid subtraction scintigraphy. *J Nucl Med* 1993;34:24–29.
20. Kume N, Suga K, Nishiguchi K, Camaro M, Matsunaga N. Relationship between thallium-201 and tumor proliferative activity in thyroid nodules *Eur J Nucl Med* 1996;23:376–382.
21. Bravo R, Flank R, Lundell PA, MacDonald-Bravo H. Cyclin/PCNA is the auxiliary protein of DNA polymerase δ. *Nature* 1987;326:515–517.
22. Ogata K, Kurki PO, Celis JE, Nakamura RM, Tan EM. Monoclonal antibodies to a nuclear protein associated with DNA replication. *Exp Cell Res* 1987;168:475–486.
23. Galand P, Degraef C. Cyclin/PCNA immunostaining as an alternative to tritiated thymidine pulse labeling for marking S phase cells in paraffin sections from animal and human tissues. *Cell Tissue Kinet* 1989;22:383–392.
24. Camplejohn RS, Ash CM, Gillett CE, et al. The prognostic significance of DNA flow cytometry in breast cancer: results in 881 patients treated in a single center. *Br J Cancer* 1995;71:140–145.
25. Silvestrini R, SICCAB Group for Quality Control of Cell Kinetic Determinations. Quality control for evaluation of the S-phase fraction by flow cytometry: a multicentric study. *Cytometry* 1994;18:11–16.
26. Sinclair WK. Cyclic x-ray responses in mammalian cells in vitro. *Radiat Res* 1968;33:620–643.
27. Sinclair WK, Morton RA. X-ray sensitivity during the cell generation cycle of cultured Chinese hamster cells. *Radiat Res* 1966;29:450–474.

Fluorine-18-Fluorodeoxyglucose Assessment of Glucose Metabolism in Bone Tumors

Annemieke C. Kole, Omgo E. Nieweg, Harald J. Hoekstra, James R. van Horn, Heimen Schraffordt Koops and Willem Vaalburg

PET Center, Departments of Surgical Oncology and Orthopedic Surgery, Groningen University Hospital, Groningen; Department of Surgery, The Netherlands Cancer Institute, Amsterdam, the Netherlands

In our study, we investigate the glucose metabolism of various types of bone lesions with ^{18}F-fluorodeoxyglucose (FDG) PET. **Methods:** Twenty-six patients showing clinical and radiographic symptoms of a malignant bone tumor were included. Histological examination after the PET study revealed 19 malignant and 7 benign tumors. PET images were corrected for attenuation. Arterial blood samples were taken to establish the input function. The metabolic rate of glucose consumption (MRglc) was calculated for the whole tumor, for the 10 pixels with maximum activity and for contralateral normal muscle tissue. **Results:** All lesions were clearly visualized with ^{18}F-FDG PET except for a small infarction of the humerus. All the other lesions had increased glucose metabolism compared to surrounding and contralateral muscle tissue. Both maximum and average MRglc for benign, as well as malignant, lesions were significantly higher than for contralateral normal tissue. The maximum and average MRglc were not higher for malignant as opposed to benign lesions. There was a large overlap between the MRglc of benign and malignant lesions. **Conclusion:** Fluorine-18-FDG PET appears suitable to visualize bone tumors. With the quantification of glucose metabolism, it is not possible to differentiate between benign and malignant bone tumors. There does not seem to be a clear correlation between the MRglc and the biologic aggressiveness of the neoplasms.

Key Words: bone neoplasms; glucose metabolism; PET; fluorine-18-fluorodeoxyglucose

J Nucl Med 1998; 39:810–815

Received Mar. 19, 1997; revision accepted Aug. 5, 1997.

For correspondence or reprints contact: Annemieke C. Kole, MD, PET Center and Department of Surgical Oncology, Groningen University Hospital, P.O. Box 30.001, 9700 RB Groningen, the Netherlands.

PET offers the possibility of investigating the metabolism of tumors in vivo with radiopharmaceuticals. Fluorine-18-fluorodeoxyglucose (FDG) is a well-known tracer. It behaves in vivo like glucose up to its phosphorylization inside the cell. Fluorine-18-FDG is trapped inside the cell because its metabolite, ^{18}F-FDG-phosphate, is neither a substrate for glucose-6-phosphatase nor for fructose-6-phosphatase. In tissues with high glucose consumption, more ^{18}F-FDG is taken up. Malignant neoplasms have an increased glucose consumption (*1*) The potential of PET with ^{18}F-FDG to visualize various types of tumors is well established (*2–5*).

High glucose consumption measurements determined with PET have been described in several types of soft-tissue sarcoma (*6–8*). With ^{18}F-FDG PET, benign lesions can often be distinguished from malignant ones. The relationship between the glucose metabolism of soft-tissue sarcomas, as measured with PET, and the malignancy grade has been shown (*8,9*). However, little is known about the glucose metabolism of bone tumors. Our current study uses ^{18}F-FDG PET to investigate the glucose consumption in patients with various types of bone lesions.

MATERIALS AND METHODS

Patients

Twenty-six patients (9 women, 17 men; age range 15–65 yr; mean age 31 yr) who had clinical and radiographic malignant bone tumor symptoms were studied. Conventional imaging for these patients consisted of radiography, CT and bone scintigraphy. A biopsy to obtain a definite diagnosis was performed in all patients, after the PET study, in order to avoid the interference of glucose metabolism with wound healing. Histological examination revealed 19 malignant and 7 benign tumors. Patient characteristics are presented in Table 1. Patients had not received any cancer therapy before the PET study. The study protocol was approved by the Medical Ethics Committee of the Groningen University Hospital. All patients gave informed consent.

PET Studies

Fluorine-18-FDG, with a radiochemical purity of more than 98%, was produced routinely by a robotic system according to the procedure described by Hamacher (*10*). A 951/31 ECAT positron scanner (Siemens/CTI, Knoxville, TN) was used for data acquisition. The scanner acquires 31 contiguous tomographic slices simultaneously over a total axial length of 10.8 cm.

Before the PET study, patients fasted overnight and also had their normal plasma glucose levels (mean 90 mg/dl, range 72–119) measured. A 20-gauge needle was inserted into the radial artery under local anesthesia. An intravenous cannula was inserted into the cephalic vein for the ^{18}F-FDG injection. The patients were in a supine position in the scanner with the bone lesion in the field of view. A 20-min transmission scan was obtained to correct for attenuation of the photons by the body tissues. Then, 370 MBq (10 mCi) ^{18}F-FDG was intravenously administered and dynamic images were acquired at the lesion level by obtaining 16 frames from the time of injection through 50 min postinjection. These include ten 30-sec frames, three 5-min frames and three 10-min frames. To establish the input function, 2-cc blood samples were taken simultaneously from the arterial canula (at 0.25, 0.5, 0.75, 1, 1.25, 1.5, 1.75, 2.25, 2.75, 3.75, 4.75, 7.5, 12.5, 17.5, 25, 35 and 45 min after injection). Samples were centrifuged and the plasma activity was assessed using a well counter.

TABLE 1
Patient Characteristics and Fluorine-18-FDG PET Results

Patient No.	Sex	Age (yr)	Histology	Localization	Volume (ml)	Malignant	MRglc			SUV		
							Average	Maximum	Control	Average	Maximum	Control
1	F	19	Osteogenic sarcoma	Femur	160	+	15.2	65.0	1.5	2.73	9.08	0.41
2	M	24	Osteogenic sarcoma	Knee joint	213	+	6.9	13.9	1.7	1.59	2.93	0.45
3	M	21	Osteogenic sarcoma	Humerus	60	+	10.2	21.7	2.5	1.86	3.52	0.53
4	F	17	Osteogenic sarcoma	Tibia	205	+	10.0	24.0	3.0	1.91	3.46	0.51
5	M	20	Osteogenic sarcoma	Humerus	141	+	9.7	21.9	3.0	2.07	4.17	0.80
6	M	16	Mesenchymal chondrosarcoma	Tibia	178	+	6.9	13.7	1.4	1.80	3.36	0.51
7	M	19	Chondrosarcoma grade III	Sacroiliac joint	*	+	16.8	62.7	3.3			
8	M	23	Primitive neuroectodermal tumor	Humerus	51	+	11.0	19.3	2.3			
9	M	26	Ewing's sarcoma	Femur	85	+	8.3	22.2	1.3	1.75	3.54	0.41
10	M	18	Ewing's sarcoma	Femur	203	+	5.5	15.2	1.1	1.48	3.41	0.35
11	F	50	Malignant fibrous histiocytoma	Ilium	225	+	58.4	122.1	2.4	2.96	5.73	0.22
12	M	65	Malignant fibrous histiocytoma	Pubic bone	300	+	60.5	147.7	5.2	6.93	16.06	0.68
13	M	22	Malignant lymphoma of bone	Tibia	252	+	51.4	113.7	2.4	5.55	11.36	0.51
14	M	58	Malignant lymphoma of bone	Knee joint	62	+	55.6	101.0	2.1	7.57	13.65	0.51
15	F	58	Metastasis renal carcinoma	Femur	9	+	36.2	102.1	2.0	3.60	9.17	0.37
16	M	42	Metastasis adenocarcinoma lung	Ischium	373	+	19.0	39.0	1.1	3.39	6.53	0.52
17	M	36	Metastasis adenocarcinoma lung	Ischium	64	+	31.1	65.6	1.6	6.28	12.51	0.53
18	F	48	Metastasis squamous cell carcinoma from unknown origin	Ilium	265	+	38.1	69.0	2.7	7.64	13.29	0.74
19	M	56	Myeloma (M. Kahler)	Ilium	1014	+	13.6	38.4	2.7	2.71	5.44	0.63
20	F	35	Osteoblastoma	Tibia	59	−	9.5	38.1	1.6	3.28	8.70	0.49
21	M	15	Myositis (S. aureus)	Femur	354	−	17.9	40.5	1.6			
22	F	15	Juxtacortical chondroma	Fibula	11	−	5.6	10.3	2.7	4.04	4.94	0.28
23	F	21	Myositis ossificans	Ilium	73	−	7.8	16.1	2.2	1.36	2.23	0.57
24	M	38	Bone infarction	Humerus	†	−	2.3	†	1.9	0.71	†	0.63
25	M	18	Aneurysmatic bone cyst	Tibia	105	−	12.3	27.9	2.0	2.69	5.15	0.51
26	F	18	Fibrous dysplasia	Parietal bone	29	−	12.9	28.4	5.7	2.18	12.27	1.07

*Tumor largely exceeded field of view.
†Could not be established.

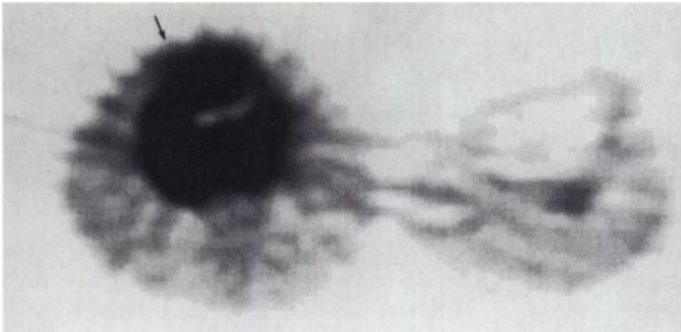

FIGURE 1. Transversal PET image of the knees of a 58-yr-old man with a large-cell B-cell lymphoma of bone (Patient 14).

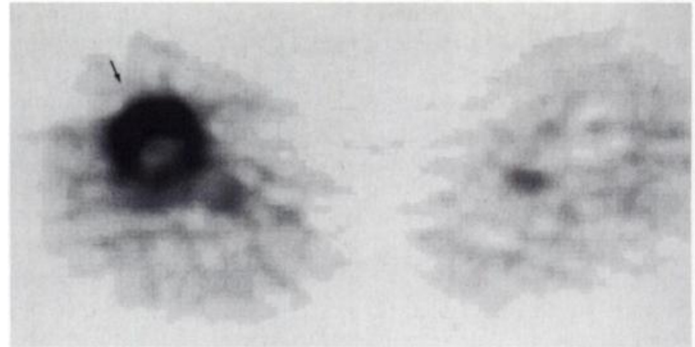

FIGURE 2. PET image of the upper legs of a 58-yr-old woman with a bone lesion that proved to be a metastasis of a renal cell carcinoma (Patient 15).

Data Analysis

The circumference of the lesion was outlined with the aid of dedicated software developed at our institution and described previously (*11*). This software uses a manually chosen threshold technique to define tissue with increased activity after masking all nonpathologic tissue with high activity. The threshold is chosen on the last frame of the dynamic study by combining the data of all planes. Using this technique, all involved tissue in the field of view is defined and its volume is calculated automatically. The activity in the selected pixels is averaged and the corresponding time-activity curve is calculated. By combining the averaged time-activity data with the plasma input data, the average metabolic rate of glucose consumption (MRglc) in Fmol/100 g tumor tissue/min was calculated using the Patlak analysis. Since the lumped constant of tumor tissue is unknown, the lumped constant of 0.42 of normal brain tissue was used (*12,13*). By calculating the MRglc for the 10 pixels with highest activity, the maximum MRglc of the pathologic process was also obtained. By using this method, the partial volume effect is made smaller, because the count density in adjacent structures will have a less disturbing influence on the ultimate MRglc value. When the lesion could not be visualized clearly, a region of interest (ROI) was drawn around its location based on MRI or CT findings. The MRglc in contralateral normal tissue was also calculated using an ROI technique. Because normal bone tissue has an extremely low glucose metabolism, and drawing an ROI around something you can only locate due to its absence is difficult, the contralateral ROIs were drawn in muscle tissue. In addition to the MRglc, standardized uptake values (SUV) were calculated with the following equation:

$$\text{SUV} = \frac{\text{tissue concentration (MBq/g)}}{\text{injected dose (MBq)/body weight (g)}}$$

Statistical Analysis

Statistical analysis included the Student's t-test to test the hypothesis that there is a difference between the MRglc values of benign and malignant lesions. The paired Student's t-test was used to compare the MRglc in tumor tissue to that in the corresponding contralateral normal tissue. A p value of < 0.05 was considered significant.

RESULTS

All lesions were clearly visualized with ^{18}F-FDG PET except for a small infarction of the humerus (2 cm on conventional imaging). All the other lesions had increased glucose metabolism compared to surrounding and contralateral normal tissue. Particularly high MRglc was seen in the malignant fibrous histiocytoma, malignant lymphoma (Fig. 1) and in the metastatic lesions (Fig. 2), whereas glucose consumption was substantially lower in other neoplasms such as osteogenic and Ewing's sarcoma (Fig. 3) and benign lesions such as juxtacortical chondroma and myositis ossificans (Fig. 4).

The mean of all patients' average MRglc of tumor tissue was 20.5 μmol/100 g/min (range 2.3–60.5) and the mean of the MRglc maximums was 49.6 μmol/100 g/min (range 10.3–147.8). The mean MRglc of contralateral normal muscle tissue was 2.3 μmol/100 g/min (range 1.1–5.7). The mean of the average SUVs of tumor tissue was 3.20 (range 0.74–7.64) and the mean of the maximum SUVs was 7.07 (range 2.23–16.06). The mean SUV of contralateral normal muscle tissue was 0.53 (range 0.22–1.07). The MRglc and the SUV for benign and malignant lesions were significantly higher than for contralateral normal tissue. The maximum and average MRglc and the

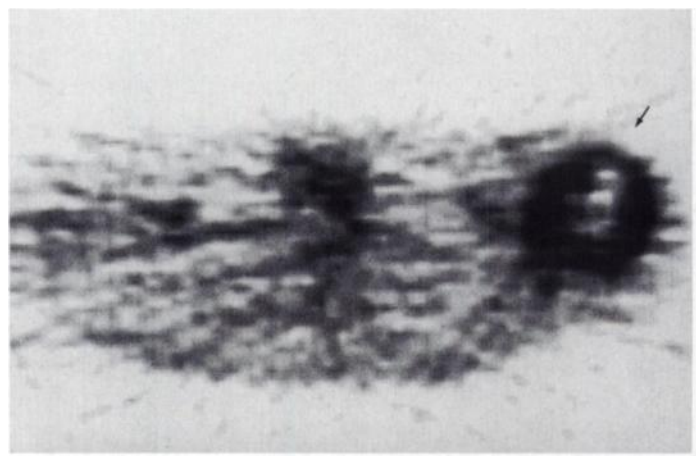

FIGURE 3. PET image of the upper part of the thorax of a 20-yr-old man with an osteogenic sarcoma of the humerus (Patient 5).

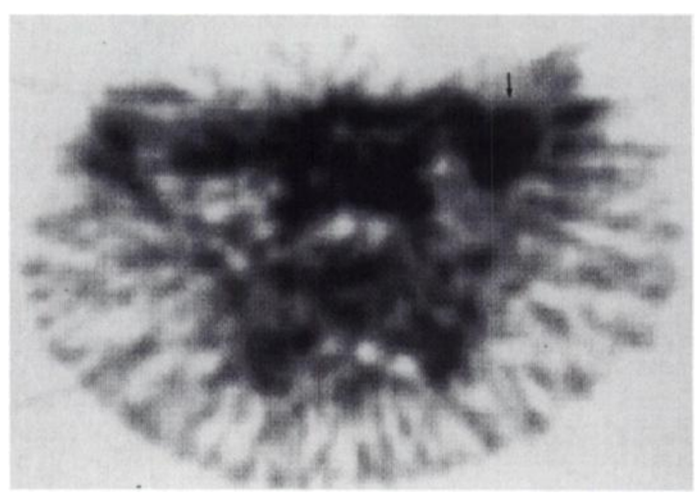

FIGURE 4. PET image of the pelvis of a 21-yr-old woman with a bone lesion that later appeared to be caused by myositis ossificans (Patient 23).

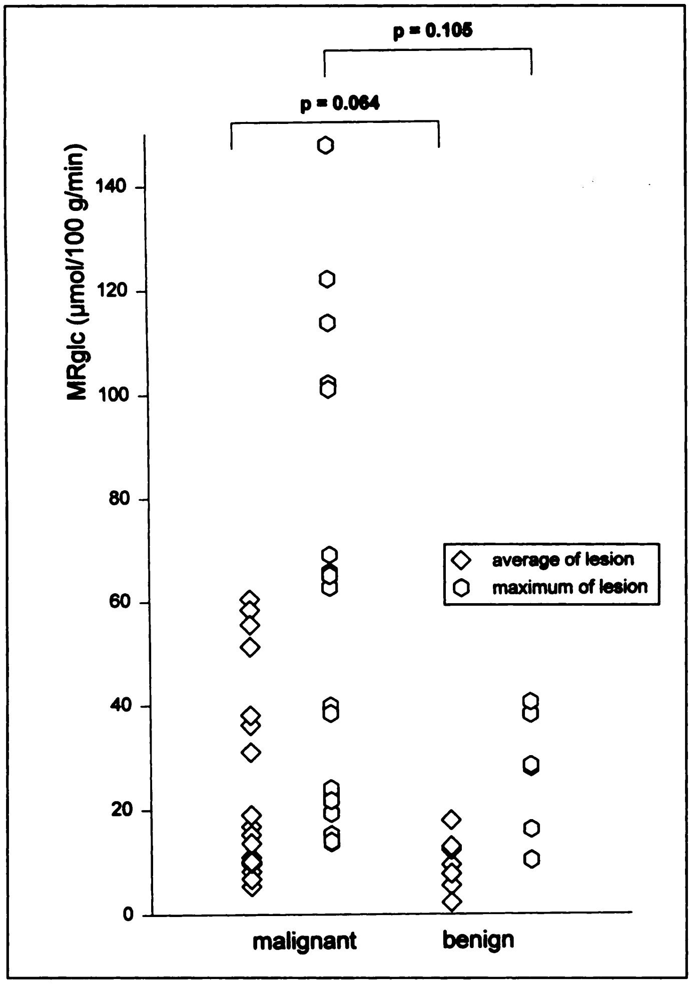

FIGURE 5. Average and maximum MRglc of all bone lesions studied. There appeared no significant difference in MRglc between benign and malignant lesions.

SUVs were not significantly different for malignant and benign lesions (Fig. 5). There was a large overlap between the MRglc and the SUV of benign and malignant lesions, such that receiver operating characteristic (ROC) analysis could not provide an acceptable cutoff point for discrimination (Fig. 6). An accurate discrimination by time-activity-curve analysis was not feasible either. However, all lesions with a maximum MRglc > 40.5 μmol/100 g/min or an average MRglc > 17.9 μmol/100 g/min were malignant. The same is valid for lesions with a maximum SUV > 12.27 or an average SUV > 4.04.

DISCUSSION

Our study shows that PET with the glucose analog ^{18}F-FDG can visualize benign as well as malignant bone lesions. PET offers in vivo a visible and quantifiable insight into a metabolic process for a skeletal disease. On the other hand, the clinical significance of these findings is not immediately apparent. Techniques such as radiographs, CT and MRI depict the anatomic detail that PET images lack. Bone scintigraphy is a far simpler technique to demonstrate skeletal abnormalities and may be at least as sensitive. The fact that both benign and malignant lesions are depicted equally well indicates that the rate of glucose metabolism is similar in benign and malignant lesions and does not separate them. In contrast to the findings in soft-tissue sarcomas, there does not seem to be a correlation between the MRglc and the biologic aggressiveness of the neoplasms. These results do not correspond with the findings from Dehdashti et al. (*14*) who found that ^{18}F-FDG PET

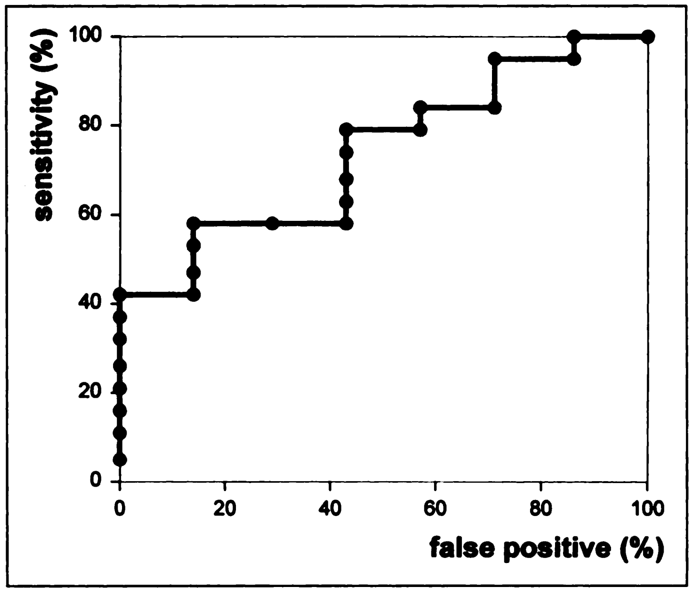

FIGURE 6. Receiver operating characteristic (ROC) curve of ^{18}F-FDG PET for bone tumors. When test values are measured on a continuum, sensitivity and specificity levels depend on where the cutoff between positive and negative is set. The closer an ROC curve is to the upper left-hand corner of the graph, the more accurate it is, because the sensitivity approaches 100% without false-positive results. There was no acceptable cutoff point for this indication.

demonstrates a clear distinction between benign and malignant intraosseous lesions. However, they investigated only 3 primary bone tumors and 12 metastatic lesions, so their patient group is not representative for patients with primary bone tumors.

In the evaluation of a variety of tumors, ^{18}F-FDG PET has proved to be a valuable adjunct to other imaging modalities. For instance, malignant myeloma was clearly depicted on the PET images (Fig. 7). These patients often have a negative bone scan with ^{99m}Tc-phosphate possibly due to the production of an osteoclast-activating factor that promotes bone resorption without osteoblastic change (*15,16*). Several types of metastatic lesions are also invisible using conventional bone scintigraphy (*17,18*). The use of ^{18}F-FDG PET is based primarily on the observation that malignant tumors have increased glycolysis compared to normal tissues (*19*). Proposed explanations for this phenomenon include increased concentration of hexokinase in malignant cells, which results in a higher uptake and phosphorylation of glucose (and FDG) and increased amounts of a special glucose transporter in malignant cells, which results in a higher rate of entry of glucose (and FDG) (*20,21*). However, the relation of these features to malignancy grade has not yet

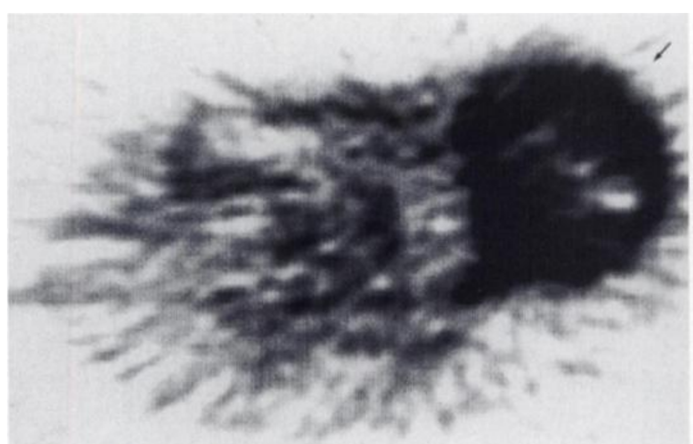

FIGURE 7. PET image of the pelvis of a 56-yr-old man with a malignant myeloma (Patient 19).

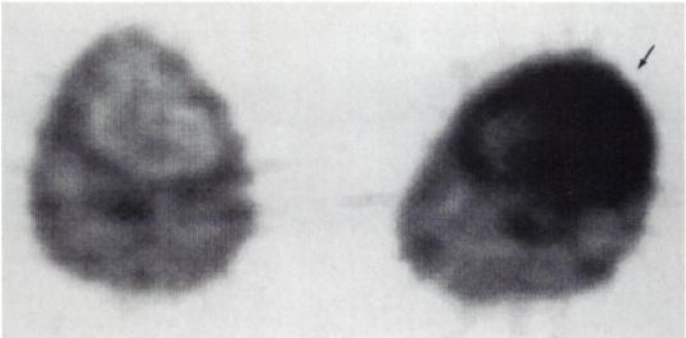

FIGURE 8. PET image of the proximal part of the lower legs of an 18-yr-old man with an aneurysmatic bone cyst (Patient 25).

been elucidated. In brain tumors, both positive and negative correlations have been demonstrated (*22,23*).

It has been suggested that hyperglycemia may increase the sensitivity of tumor tissue to therapy (*24,25*). The more metabolically active the cell at the time of exposure to cytotoxic treatment or radiation therapy, then the higher the possibility that the DNA is more susceptible to damage and, therefore, the more effective the treatment (*26*). Evidence exists to support this hypothesis. A recent PET study in patients with soft tissue sarcoma indicated that predicting the treatment outcome based on pretreatment glucose consumption is possible (*28*). In our study, all four of the patients with osteogenic sarcoma, with relatively low MRglc (Patients 2–5), did respond poorly to the subsequent chemotherapy, whereas the one patient with higher MRglc (Patient 1) responded well to therapy.

Little has been published about PET in benign lesions. It is known that inflammatory lesions such as arthritis and sarcoidosis show increased ^{18}F-FDG uptake (*28,29*) probably due to the metabolic activity of macrophages and granulation tissue (*30*). The aneurysmal bone cyst may be a reparative process as the result of trauma or tumor induced anomalous vascular process (*31*). The metabolic activity as established with ^{18}F-FDG PET validates this theory (Fig. 8). Osteoblastoma is marked by very active formation of osteoid and immature bone trabeculae produced by compact masses of hypertrophic osteoblasts (*32*). There can even be an inflammatory response to osteoblastoma (*33*). This metabolic activity is most likely responsible for the increased ^{18}F-FDG uptake that we found (Fig. 9).

PET offers interesting options for further research. Other radiopharmaceuticals may be developed to distinguish benign from malignant lesions. The affinity of the positron-emitting ^{18}F may be exploited for bone imaging. PET can detect the local recurrence of a tumor in the early phase, since metabolic changes precede anatomic changes particularly in the area that has been treated previously. PET with ^{18}F-FDG has the potential as an agent to monitor the effects of chemotherapy. Radiographic imaging techniques are notoriously insensitive for evaluating the effects of treatment, since anatomic changes lag behind metabolic changes. When chemotherapy or radiotherapy influences the level of glucose consumption, this is immediately reflected in the MRglc in tumor cells as measured by PET. Research in this direction is in progress (*34*). In addition to the possibility of quantifying metabolism, ^{18}F-FDG PET may have another advantage over ^{99m}Tc-phosphate bone scanning, since the biological basis of the latter technique is that it reflects osteoblast activity rather than tumor metabolism per se. Fluorine-18-FDG is presumed to be associated with the metabolic activity of the tumor itself (*17,18*).

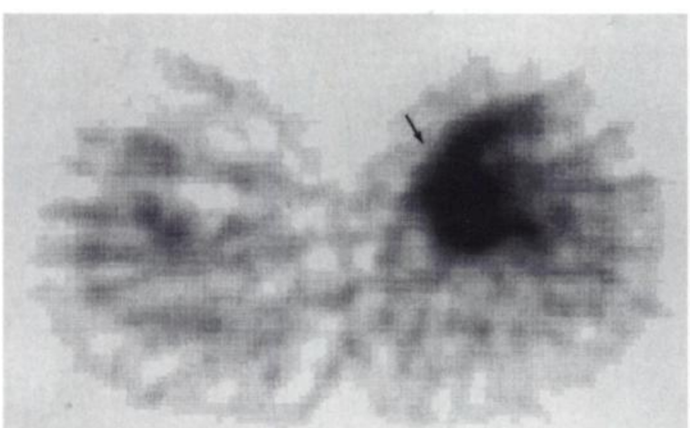

FIGURE 9. PET image of the lower legs of a 35-yr-old woman with an osteoblastoma of the tibia (Patient 20).

CONCLUSION

Fluorine-18-FDG PET appears suitable for visualizing bone tumors, but with the quantification of glucose metabolism, it is not possible to differentiate between benign and malignant bone tumors, although the lesions with the highest glucose utilization were all malignant.

ACKNOWLEDGMENTS

Financial support was provided by the Dutch Cancer Society (Koningin Wilhelmina Fonds, Grant RuG 94-786). We also thank A.T.M. Willemsen for his help with the data analysis.

REFERENCES

1. Warburg O. On the origin of cancer cells. *Science* 1956;123:309–314.
2. Leskinen-Kallio S. Positron emission tomography in oncology. *Clin Physiol* 1994;14:329–335.
3. Shields AF, Graham MM, Spence AM. The role of PET imaging in clinical oncology. A current status report. In: Freeman LM, ed. *Nuclear medicine annual.* New York: Raven Press; 1995:129–168.
4. Jones T. The imaging science of positron emission tomography. *Eur J Nucl Med* 1996;23:807–813.
5. Lamki LM. Positron emission tomography in oncology. *Cancer* 1996;78:2039–2042.
6. Kern KA, Brunetti A, Norton JA, et al. Metabolic imaging of human extremity musculoskeletal tumors by PET. *J Nucl Med* 1988;29:181–186.
7. Griffeth LK, Dehdashti F, McGuire AH, et al. PET evaluation of soft-tissue masses with fluorine-18 fluoro-2-deoxy-D-glucose. *Radiology* 1992;182:185–194.
8. Adler LP, Blair HF, Makley JT, et al. Noninvasive grading of musculoskeletal tumors using PET. *J Nucl Med* 1991;32:1508–1512.
9. Nieweg OE, Pruim J, van Ginkel RJ, et al. Fluorine-18-fluorodeoxyglucose PET imaging of soft-tissue sarcoma. *J Nucl Med* 1996;37:257–261.
10. Hamacher K, Coenen HH, Stocklin G. Efficient stereospecific synthesis of no-carrier-added ^{18}F-fluoro-2-deoxy-D-glucose using aminopolyether supported nucleophilic substitution. *J Nucl Med* 1986;27:235–238.
11. Kole AC, Nieweg OE, Pruim J, et al. Standardized uptake values and the quantification of metabolism with FDG and L-[1-^{11}C]-tyrosine PET in patients with breast cancer. *J Nucl Med* 1997;38:692–696.
12. Patlak CS, Blasberg RG, Fenstermacher JD. Graphical evaluation of blood-to-brain transfer constants from multiple-time uptake data. *J Cereb Blood Flow Metab* 1983;3:1–7.
13. Patlak CS, Blasberg RG. Graphical evaluation of blood-to-brain transfer constants from multiple-time data. Generalizations. *J Cereb Blood Flow Metab* 1985;5:584–590.
14. Dehdashti F, Siegel BA, Griffeth LK, et al. Benign versus malignant intraosseous lesions: discrimination by means of PET with 2-[^{18}F]-fluoro-2-deoxy-D-glucose. *Radiology* 1996;200:243–247.
15. Mundy GR, Raisz LG, Cooper RA, Schechter GP, Salmon SE. Evidence for the secretion of an osteoclast stimulating factor in myeloma. *N Engl J Med* 1974;291:1041–1046.
16. Woolfenden JM, Pitt MJ, Durie BGM, Moon TE. Comparison of bone scintigraphy and radiography in multiple myeloma. *Radiology* 1980;134:723–728.
17. Sasaki M, Ichiya Y, Kuwabara Y, et al. Fluorine-18-fluorodeoxyglucose positron emission tomography in technetium-99m-hydroxymethylenediphosphate negative bone tumors. *J Nucl Med* 1993;34:288–290.
18. Vieras F, Herzberg DL. Focal decreased skeletal uptake secondary to metastatic disease. *Radiology* 1976;118:121–122.
19. Warburg O. *The metabolism of tumors.* New York: Richard R. Smith; 1931:129.
20. Brown RS, Wahl RL. Overexpression of Glut-1 glucose transporter in human breast cancer. An immunohistochemical study. *Cancer* 1993;72:2979–2985.
21. Hiraki Y, Rosen OM, Birnbaum MJ. Growth factors rapidly induce expression of glucose transporter gene. *J Biol Chem* 1988;27:13655–13662.

22. Kornblith PL, Cummings CJ, Smith BH, Brooks RA, Patronas NJ, Di Chiro G. Correlation of experimental and clinical studies of metabolism by PET scanning. *Prog Exp Tumor Res* 1984;27:170–178.
23. Lowry OH, Berger SJ, Carter JG, et al. Diversity of metabolic patterns in human brain tumors: enzymes of energy metabolism and related metabolites and cofactors. *J Neurochem* 1983;41:994–1010.
24. Fradkin SZ, Zhavrid EA, Nebyshinskaia NS, Istomin IuP. Induced hyperglycemia as a factor of modification of sarcoma 45 sensitivity to chemotherapy [English Abstract]. *Eksp Onkol* 1987;9:64–68.
25. Krimker VM, Goldobenko GV, Ozhiganov EL, Aitakova TI, Diuskaliev ZhD. The use of artificial hyperglycemia in the radiotherapy of patients with rectal cancer [English Abstract]. *Eksp Onkol* 1986;32:40–46.
26. Tayek JA. A review of cancer cachexia and abnormal glucose metabolism in humans with cancer. *J Am Coll Nutr* 1992;11:445–456.
27. Van Ginkel RJ, Hoekstra HJ, Pruim J, et al. FDG-PET to evaluate response to hyperthermic isolated limb perfusion for locally advanced soft-tissue sarcoma. *J Nucl Med* 1996;37:984–990.
28. Palmer WE, Rosenthal DI, Schoenberg OI, et al. Quantification of inflammation in the wrist with gadolinium-enhanced MR imaging and PET with 2-[^{18}F]-fluoro-2-deoxy-D-glucose. *Radiology* 1995;196:647–655.
29. Brudin LH, Valind SO, Rhodes CG, et al. Fluorine-18 deoxyglucose uptake in sarcoidosis measured with positron emission tomography. *Eur J Nucl Med* 1994;21:297–305.
30. Kubota R, Yamada S, Kubota K, Ishiwata K, Tamahashi T, Ido T. Intratumoral distribution of fluorine-18-fluorodeoxyglucose in vivo: high accumulation in macrophages and granulation tissues studied by microautoradiography. *J Nucl Med* 1992;33:1972–1980.
31. Kransdorf MJ, Sweet DE. Aneurysmal bone cyst: concept, controversy, clinical presentation, and imaging. *Am J Roentgenol* 1995;164:573–580.
32. Schajowicz F, Lemos C. Osteoid osteoma and osteoblastoma: closely related entities of osteoblastic derivation. *Acta Orthop Scand* 1970;41:272–291.
33. Crim JR, Mirra JM, Eckardt JJ, Seeger LL. Widespread inflammatory response to osteoblastoma: the flare phenomenon. *Radiology* 1990;177:835–836.
34. Brecht-Krauss D, Guhlman CA, Schulte M, Glatting G, Kinzl L, Reske SN. Monitoring chemotherapy response in osteosarcoma by [^{18}F]FDG-PET [Abstract]. *Eur J Nucl Med* 1996;23:1104.

FDG PET for Detection and Therapy Control of Metastatic Germ Cell Tumor

Uwe Cremerius, Peter J. Effert, Gerhard Adam, Osama Sabri, Michael Zimny, Gudrun Wagenknecht, Gerhard Jakse and Udalrich Buell

Departments of Nuclear Medicine, Urology and Diagnostic Radiology, University Hospital, Aachen University of Technology, Aachen, Germany

We investigated the use of PET and 2[^{18}F]fluoro-2-deoxy-D-glucose (FDG) for detection and therapy control of metastatic germ cell cancer in comparison to CT. **Methods:** Fifty-four PET studies were performed in addition to CT in 33 patients with histopathologically proven germ cell tumors (14 seminomas, 18 nonseminomas, 1 not classified). The scans were done either after initial diagnosis (Group 1; n = 12), within 2 wk after completion of chemotherapy (Group 2; n = 13) or 14–375 days after chemotherapy (Group 3; n = 29). PET and CT were validated either by histology (n = 19) or clinical follow-up for 182–1704 days (n = 35). Focal pathological uptake with PET was quantified using standardized uptake values (SUVs). **Results:** PET was significantly more accurate than CT (0.86 versus 0.59; $p < 0.025$) for detection of residual viable tumor in Group 3. While sensitivities of PET and CT did not differ markedly, PET was significantly more specific than CT. No significant differences between PET and CT were found in Groups 1 and 2. PET scans after therapy resulted in false-negative findings in five of nine cases of Group 2 but only in two of nine cases of Group 3. False-positive PET findings occurred in three inflammatory processes. SUV of seminomas was significantly higher than in nonseminomas ($p < 0.01$). **Conclusion:** PET using FDG is superior to CT for assessment of residual tumor after chemotherapy of germ cell cancer and may thus have an increased effect on patient management in the future. PET must be performed at least 2 wk after completion of therapy. Further data are necessary to determine the role of FDG PET for initial staging of germ cell cancer.

Key Words: germ cell tumor; staging; therapy control; PET; fluorine-18-fluorodeoxyglucose

J Nucl Med 1998; 39:815–822

Testicular cancer is now the most frequent malignancy among men between 20 yr and 40 yr. Incidences of 4–10 of 100000 have been reported in most industrialized countries (*1*). Germinal cell tumors are categorized into pure seminomas (40%) and into the heterogeneous group of nonseminomatous tumors comprising teratoma, chorionic carcinoma, embryonal and mixed or combination tumors (*2*).

Metastatic spread is found in 70% of nonseminomatous tumors and 30% of seminomas at the time of diagnosis. With radiotherapy and the introduction of cisplatin combination chemotherapy, prognosis of metastatic testicular cancer has been dramatically improved. Cure rates of 80%–90% were reported in Stage II and III patients; cure is also possible in patients who failed to achieve complete remission after initial therapy (*3*).

Staging after initial diagnosis determines whether systemic chemotherapy, abdominal radiotherapy or no further therapy is necessary. Diagnosis of metastatic spread is usually made by CT of abdomen and chest and/or elevated tumor markers (human chorionic gonadotropin (HCG), alpha-fetoprotein (AFP) and lactate dehydrogenase). CT-based clinical staging has been shown to have a false-negative rate in clinical Stage I patients of 30%–40% even with third- and fourth-generation CT scanners (*4,5*). As a consequence, Stage I seminomas undergo abdominal radiation therapy, whereas different therapeutic strategies are presently performed in clinical Stage I nonseminomas. These strategies comprise retroperitoneal lymph node dissection (RPLND), chemotherapy or surveillance. Due to excellent cure rates in early testicular cancer, therapy-induced morbidity (disturbances of ejaculation, infertility, surgical complications, induction of secondary tumors) has become an important matter. The development of better noninvasive imaging techniques would be a key to a more individualized therapy.

Another problematic issue is the occurrence of indeterminate residual masses in CT after completion of chemotherapy in 15%–75% of patients. Surgical resection of the mass is usually performed and histological examination shows necrosis/fibrosis in 40%–50% of the cases, differentiated teratoma in 12%–40% of the cases and persistent viable malignancy in 20%–40% of

Received Apr. 1, 1997; revision accepted Jul. 4, 1997.

For correspondence or reprints contact: Uwe Cremerius, MD, Department of Nuclear Medicine, University Hospital, Pauwelsstr. 30, D-52057 Aachen, Germany.